

A robotic goniometer exchanger for high-throughput single-crystal X-ray diffraction at SPring-8

Yuiga Nakamura,* Sumit Ranjan Maity, Toshiyuki Sasaki and Kouhei Ichiyanagi

Japan Synchrotron Radiation Research Institute (JASRI), 1-1-1 Kouto, Sayo-cho, Sayo-gun, Hyōgo 679-5198, Japan.

*Correspondence e-mail: ynakamura@spring8.or.jp

Received 30 October 2025

Accepted 25 February 2026

Edited by M. Retegan, ESRF – The European Synchrotron, France

Keywords: single-crystal X-ray diffraction; robotic-arm diffractometer; synchrotron instrumentation; high-energy X-rays; automation.

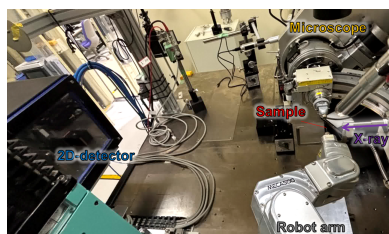
Supporting information: this article has supporting information at journals.iucr.org/s

Rapid and reliable sample handling is essential for high-throughput single-crystal diffraction at modern synchrotron facilities. At the high-energy single-crystal X-ray diffraction beamline BL02B1 of SPring-8, a compact six-axis robotic arm was implemented as a diffractometer for single-crystal measurements using high-energy X-rays. Coordinated six-axis motion enables virtual rotation about an arbitrary axis and reproduction of a conventional ω -scan geometry without additional rotary stages. Under identical beam conditions ($180\ \mu\text{m} \times 113\ \mu\text{m}$), the robotic-arm system yielded diffraction data with an internal agreement factor of $R_{\text{int}} = 0.117$, comparable with that obtained using a conventional goniometer ($R_{\text{int}} = 0.134$). Optical microscopy and diffraction analysis indicate a positional deviation of approximately $\pm 17\ \mu\text{m}$ during ω -scans, with a standard deviation of the spindle position of 0.14° . Although this accuracy is lower than that of high-precision single-crystal goniometers, it is sufficient for diffraction experiments employing large beam sizes and high-energy X-rays. Owing to its compact design, programmable motion control and open geometry, the system provides a flexible platform for automated sample handling and high-throughput diffraction experiments in support of the SPring-8-II upgrade.

1. Introduction

Single-crystal X-ray diffraction (XRD) is indispensable for elucidating the atomic and electronic structures of crystalline materials. When combined with synchrotron radiation, it enables measurements on microcrystals using intense short-wavelength X-rays and allows structural analyses with sub-angstrom precision and electron-density resolution. Consequently, synchrotron-based single-crystal XRD has become a key technique for both fundamental crystallography and functional-materials research.

The demand for high-throughput single-crystal measurements has increased rapidly with the growth of studies that require sequential data collection, such as temperature-dependent experiments, compositional series and *in situ* or time-resolved measurements. Although modern detectors and high-flux synchrotron sources enable rapid data acquisition, overall experimental efficiency remains partially constrained by manual sample alignment and goniometer operation inside the experimental hutch. Each manual adjustment interrupts measurement continuity and limits the ability to exploit the high flux and stability of advanced synchrotron sources. Developing compact, precise and automated diffractometers is therefore essential for achieving true high-throughput operation.



Published under a CC BY 4.0 licence

At beamline BL02B1 of SPring-8, such automation has become particularly relevant. BL02B1, originally developed for high-energy single-crystal diffraction and advanced structural analysis (Sugimoto *et al.*, 2010), delivers high-energy X-rays (30–50 keV) for a broad range of materials – from inorganic oxides and halides (Maity & Nakamura, 2025) to molecular and metal–organic crystals (Nakamura *et al.*, 2025) and metal–organic frameworks – supporting research that has contributed to recent Nobel Prize-winning achievements (Kitagawa, 2025). Both precision and throughput are critical for such studies. The beamline routinely supports charge-density and advanced structural analyses (Kitou *et al.*, 2023), which often require measurements on multiple samples or under multiple conditions. The combination of high flux, diverse research targets and increasing data volume underscores the need for a goniometer system capable of rapid, reproducible and potentially automated operation to shorten measurement cycles and improve experimental efficiency.

To address this need, we have developed a robotic-arm diffractometer for single-crystal experiments at BL02B1. Although several studies have reported the use of robotic arms in XRD measurements, most of them were limited to applications as sample changers (Murakami *et al.*, 2020; Lazo *et al.*, 2021). Our system employs a six-axis compact industrial robotic arm that functions as a high-precision goniometer, with potential to also serve as an automated sample exchanger and perform automatic optical centring through programmable motion control. Compared with conventional spindle-based goniometers, the robotic arm provides additional rotational degrees of freedom, customizable motion paths and flexible access geometry, while maintaining angular precision comparable to conventional instruments. Its compact design also facilitates integration with various sample environments, such as cryostreams and hot-air blowers, making it suitable for *in situ* and time-resolved studies.

Here, we present a proof-of-principle demonstration of this robotic-arm diffractometer at BL02B1. The results confirm that the system achieves goniometric precision equivalent to existing setups, while offering enhanced flexibility and extensibility. This development represents an important step toward automated and high-throughput single-crystal diffraction in the upcoming SPring-8-II era.

2. Experimental setups

A compact six-axis robotic arm (MECA500, Mecademic) (Cowden *et al.*, 2019) was installed at the single-crystal diffraction beamline BL02B1 of the SPring-8 synchrotron facility. The MECA500 is particularly suited for synchrotron applications. Its ultra-compact design (330 mm reach, 0.5 kg payload, total weight < 5 kg) and rigid aluminium body allow installation within the confined space around the beam centre, while maintaining high mechanical stability. It can accommodate an additional load of approximately 0.5 kg, allowing the installation of user-specified small sample environments or goniometers – such as gas-flow systems, pressure cells or electric/magnetic devices – for various experimental studies.

Furthermore, the system can be controlled *via* an Ethernet connection and Python scripting. A six-axis coordinated control mode enables the simultaneous operation of all six axes, allowing the sample to be virtually rotated about an arbitrary axis. This represents the most significant difference from earlier studies, in which a high-precision small rotary axis was mounted at the tip of a large robotic arm (Nurizzo *et al.*, 2016). This functionality was also utilized to reproduce the ω -scan axis used in the present study. As shown in Fig. 1, the robotic arm was positioned directly opposite the existing spindle-type goniometer to enable comparative measurements under identical beam conditions. This configuration preserved the standard beamline setup, including the crystal-viewing camera, beam stopper and optical alignment system, without requiring any modification to the infrastructure.

A two-dimensional detector PILATUS3 X CdTe 1M (Dectris) was mounted downstream of the beam to record diffraction images from both the robotic and conventional goniometers. Due to spatial constraints introduced by the comparative setup, the sample–detector distance was set to 669.6 mm, longer than the standard 130 mm configuration at BL02B1, to maintain an unobstructed scattering geometry.

For the demonstration, a single crystal of $\text{Nd}_{1.5}\text{Sr}_{0.5}\text{NiO}_4$ (Wahyudi *et al.*, 2015) was mounted on the robotic arm using a magnetic pin holder. The measurement was performed at room temperature. High-energy X-rays (40 keV, $\lambda = 0.310 \text{ \AA}$) were employed to access a broad region of reciprocal space and to mitigate the resolution limitations imposed by the experimental layout. The beam had a full width at half-maximum (FWHM) of $180 \mu\text{m}$ vertically and $113 \mu\text{m}$ horizontally. The ω -axis was rotated through 90° at a rate of 2.5° s^{-1} , yielding 180 diffraction images for both cases. Distinct diffraction peaks were observed up to the (114) reflection ($d \simeq 2.03 \text{ \AA}$), confirming that the robotic-arm goniometer provides stable orientation control and reliable diffraction data collection under standard BL02B1 operating conditions. The robot's compact form factor and high preci-

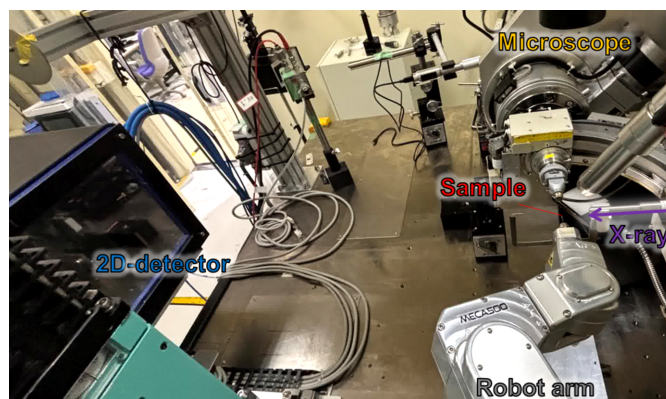


Figure 1
Experimental setup at beamline BL02B1 of SPring-8. The robotic arm (MECA500, Mecademic) was installed opposite the conventional diffractometer to allow comparative measurements under identical experimental conditions.

sion demonstrate its potential for integration into automated high-throughput diffraction workflows at SPring-8.

3. Results

Diffraction data were successfully collected using both instruments (Movies S1 and S2 of the supporting information). The robotic-arm diffractometer yielded 15 reflections (57.1% completeness), whereas the conventional goniometer produced 11 reflections (46.2% completeness). All reflections were correctly indexed, confirming the geometric accuracy of the robotic-arm setup. A slight positional fluctuation of the sample, roughly estimated to be $\sim 30\ \mu\text{m}$, was observed for the robotic-arm measurement (Fig. 2 and Movies S3 and S4), but this fluctuation did not noticeably affect the overall data quality.

To quantitatively evaluate this fluctuation, the diffraction images were processed using *CrysAlis PRO* (Rigaku OD, 2025), and the R_{int} value was employed as an indicator of internal consistency among equivalent reflections. As shown in Fig. 2, the crystal size was comparable to the beam diameter. If the positional stability of the diffractometer were insufficient, the diffraction intensity would decrease significantly during the scan, leading to an increased R_{int} value due to reduced agreement among symmetry-related intensities. Nevertheless, comparable results were obtained: $R_{\text{int}} = 0.134$ for the conventional goniometer and $R_{\text{int}} = 0.117$ for the robotic-arm diffractometer. The difference lies within experimental uncertainty. While the R_{int} values were obtained from a limited set of reflections because of constraints inherent to the experimental layout, they are sufficient to confirm that the X-ray beam did not move off the sample during the scan. In addition, we analyzed our diffraction data using the *XDS*

program (Kabsch, 2010) and calculated the ‘standard deviation of the spindle position’, which was found to be 0.14° for both the robotic-arm and the conventional diffractometers. The standard deviation of the spindle position corresponds to the deviation from the nominal rotation angle at each frame and these results suggest that the robotic-arm diffractometer has rotational speed stability comparable to that of a conventional diffractometer.

For more detailed verification, we mounted a needle at the tip of the robotic arm and quantitatively evaluated the eccentricity by tracking the position of the needle tip. For more detailed verification, an additional microscope was installed downstream of the beam, enabling simultaneous evaluation of the vertical component of the eccentricity (Fig. S1). The results obtained from the top-view and side-view microscopes at $\omega = 0, 90$ and 180° are presented (Fig. S2 and Movie S5). The eccentricity determined using the microscope positioned above the sample was $\pm 17\ \mu\text{m}$, which closely matches the value obtained from the downstream microscope. These observations indicate that the positional deviation of the robotic arm tip is approximately $\pm 17\ \mu\text{m}$ under the present experimental conditions. These findings demonstrate that the robotic-arm diffractometer achieves rotational precision and mechanical stability equivalent to a conventional single-crystal goniometer, validating its feasibility for high-energy diffraction experiments. Further refinement, such as the integration of a dedicated motorized rotation stage for the ω -axis, could further enhance angular accuracy. Even in this configuration, unlike the previously reported diffractometer (Nurizzo *et al.*, 2016), the relative orientation between the sample and the scan axis can be controlled, enabling greater flexibility in diffraction measurements. Owing to its lightweight ($\sim 5\ \text{kg}$) and modular design, such improvements and extensions toward automated sample exchange and centring can be readily implemented, paving the way for future high-throughput and autonomous diffraction measurements at SPring-8.

4. Conclusion

A proof-of-principle demonstration of a robotic-arm diffractometer has been successfully conducted at the high-energy single-crystal beamline BL02B1 of SPring-8. For applications employing X-ray beams large enough to exceed the characteristic positional deviation, the system achieves mechanical precision comparable to that of a conventional goniometer and exhibits stable diffraction performance under standard beamline conditions. Once fully implemented, this approach is expected to enable high-throughput measurements with improved space efficiency and cost effectiveness. In particular, this robotic arm could potentially be extended to function as a sample exchanger in the future, as illustrated by the initial conceptual design of the sample-exchange mechanism shown in Fig. S3. The design provides a wider χ - ϕ rotation range and can be extended to other X-ray techniques, such as thin-film diffraction or inelastic scattering. Continued development of this compact and flexible robotic platform will contribute to

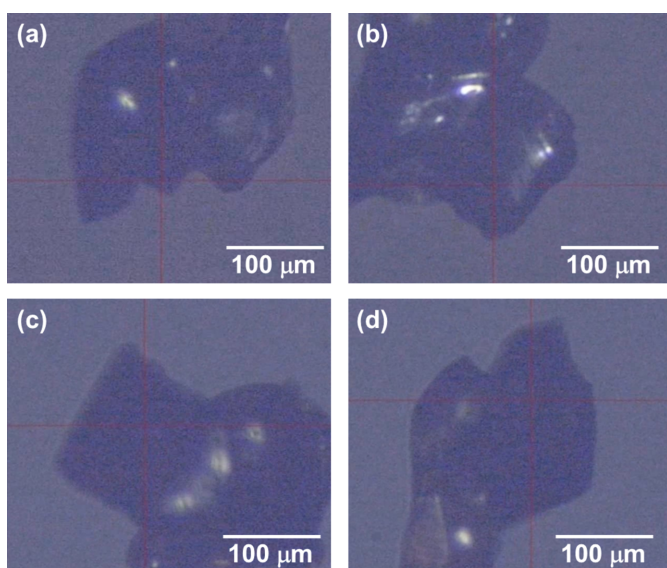


Figure 2

Crystal images obtained with the on-axis microscope of the diffractometer: (a)/(b) the robotic-arm diffractometer at $\omega = 0$ and 90° , and (c)/(d) the conventional diffractometer at $\omega = 0$ and 90° .

autonomous and efficient synchrotron experiments in the SPring-8-II era.

Acknowledgements

The XRD measurements were performed at SPring-8 with the approval of Japan Synchrotron Radiation Research Institute (JASRI) (proposal Nos. 2023B2428, 2024A1782, 2024A2337, 2024B2341, 2025A1494 and 2025A2375). The authors thank Toshiyuki Kobayashi from JASRI for assistance with the installation of the apparatus.

Conflict of interest

There are no conflicts to declare.

Data availability

Movies S1 and S2 show the diffraction patterns recorded during measurements with the robotic-arm diffractometer and the conventional goniometer, respectively. Movies S3 and S4 show microscopic views of the crystals being rotated by the robotic-arm diffractometer and the conventional goniometer, respectively. Movie S5 shows microscopic views of the needle tip mounted on the robotic arm during rotation.

Funding information

This work was supported by a KAKENHI Grant-in-Aid (Nos. 22K05054, 24K17778 and 25K18119) from the Japan Society for the Promotion of Science (JSPS) and by JASRI President Fund.

References

- Cowden, T. R., Snead, C. J., Jang, J. H. & McCubbin, F. M. (2019). *MECA500 Robotic Arm Developments Towards Astromaterials Curation Applications*. Johnson Space Center Technical Report JSC-E-DAA-TN70056. NASA Johnson Space Center, Houston, TX, USA.
- Kabsch, W. (2010). *Acta Cryst.* **D66**, 125–132.
- Kitagawa, S. (2025). *The Usefulness of the Useless – How MOFs Transformed the Concept of Porous Matter*. Nobel Prize Lecture, <https://www.nobelprize.org/prizes/chemistry/2025/kitagawa/lecture/>.
- Kitou, S., Gen, M., Nakamura, Y., Sugimoto, K., Tokunaga, Y., Ishiwata, S. & Arima, T.-H. (2023). *Adv. Sci.* **10**, 2302839.
- Lazo, E. O., Antonelli, S., Aishima, J., Bernstein, H. J., Bhogadi, D., Fuchs, M. R., Guichard, N., McSweeney, S., Myers, S., Qian, K., Schneider, D., Shea-McCarthy, G., Skinner, J., Sweet, R., Yang, L. & Jakoncic, J. (2021). *J. Synchrotron Rad.* **28**, 1649–1661.
- Maity, S. R. & Nakamura, Y. (2025). *Inorg. Chem.* **64**, 16088–16095.
- Murakami, H., Hasegawa, K., Ueno, G., Yagi, N., Yamamoto, M. & Kumasaka, T. (2020). *Acta Cryst.* **D76**, 155–165.
- Nakamura, Y., Shibayama, N., Hayashida, H., Sugimoto, K. & Miyasaka, T. (2025). *Eur. J. Inorg. Chem.* **28**, e202400682.
- Nurizzo, D., Bowler, M. W., Caserotto, H., Dobias, F., Giraud, T., Surr, J., Guichard, N., Papp, G., Guijarro, M., Mueller-Dieckmann, C., Flot, D., McSweeney, S., Cipriani, F., Theveneau, P. & Leonard, G. A. (2016). *Acta Cryst.* **D72**, 966–975.
- Rigaku OD (2025). *CrysAlis PRO*. Rigaku Corporation, Yarnton, Oxfordshire, UK.
- Sugimoto, K., Ohsumi, H., Aoyagi, S., Nishibori, E., Moriyoshi, C., Kuroiwa, Y., Sawa, H., Takata, M., Garrett, R., Gentle, I., Nugent, K. & Wilkins, S. (2010). *AIP Conf. Proc.* **1234**, 887–890.
- Wahyudi, O., Ceretti, M., Weill, I., Cousson, A., Weill, F., Meven, M., Guerre, M., Villesuzanne, A., Bassat, J.-M. & Paulus, W. (2015). *CrystEngComm* **17**, 6278–6285.